

3-D Seismic Fault Detection Using Recurrent Convolutional Neural Networks With Compound Loss

Xiao Ma, Gang Yao^{ID}, Member, IEEE, Feng Zhang, and Di Wu

Abstract—Fault detection is an essential component of seismic interpretation and plays a crucial role in industrial processes. However, it is also one of the main challenges, especially in delineating faults in 3-D seismic data. Recently, the rapidly developing technology, deep learning, has proven to be a powerful tool for this task. A number of neural networks have been proposed for this purpose by regarding 3-D fault detection as a semantic segmentation task. To further enhance the effectiveness of the deep learning methods, we propose a novel network architecture, named R2SE-Unet, to solve the 3-D segmentation problem. In the neural network, we design a recurrent residual-SE convolutional unit (RRCU-SE) that integrates the residual learning and squeeze-excitation module to store the information in 3-D seismic data. This component promotes the spread of 3-D volumetric information and aids in learning spatial dependencies in 3-D images. In addition, to reduce the impact of insufficient spatial resolution resulting from the base architecture of U-net, we add an attention unit between skip connection operations. These two new units enable our R2SE-Unet to exploit semantic information more accurately in the feature maps. After many experiments on region-based loss functions and distribution-based loss functions, we also propose a novel loss function, which takes the advantage of generalized dice (GDice) loss and balanced binary cross entropy (b-BCE) loss, named GDice-bee, to effectively train R2SE-Unet. Although only synthetic seismic data samples are used to train the network parameters, our R2SE-Unet could produce more reliable fault feature maps on field seismic data than two other conventional fault detection neural networks. Thus, the proposed neural network is easy to train and reliably works for seismic fault interpretation on field seismic data.

Index Terms—3-D fault detection, compound loss function, deep learning, field data, recurrent network.

Manuscript received 4 November 2022; revised 5 April 2023; accepted 8 May 2023. Date of publication 15 May 2023; date of current version 25 May 2023. This work was supported in part by the National Key Research and Development Program of China under Grant 2018YFA0702502, in part by the Research and Development Department of China National Petroleum Corporation (Investigations on Fundamental Experiments and Advanced Theoretical Methods in Geophysical Prospecting Applications) under Grant 2022DQ0604-02, in part by NSFC under Grant 41974142 and Grant 42074129, in part by the Science Foundation of China University of Petroleum (Beijing) under Grant 2462020YXZZ005, and in part by the State Key Laboratory of Petroleum Resources and Prospecting under Grant PRP/indep-4-2012. (*Corresponding author: Gang Yao*)

Xiao Ma, Feng Zhang, and Di Wu are with the State Key Laboratory of Petroleum Resources and Prospecting and the College of Geophysics, China University of Petroleum (Beijing), Beijing 102249, China (e-mail: mx297759805@163.com; zhangfeng@cup.edu.cn; wudi@cup.edu.cn).

Gang Yao is with the State Key Laboratory of Petroleum Resources and Prospecting and the Unconventional Petroleum Research Institute, China University of Petroleum (Beijing), Beijing 102249, China (e-mail: yao-gang@cup.edu.cn).

Digital Object Identifier 10.1109/TGRS.2023.3275951

I. INTRODUCTION

Faults are an important geotectonic feature formed by the brittle deformation of subsurface rock formations under the action of compressional or tensile forces [1]. Fault detection and interpretation are essential in understanding the underground structure and reservoir locations from seismic profiles and are crucial to geological hazard prevention and control. In seismic migration images, faults are usually depicted as lateral discontinuities. Traditional fault detection methods analyze and calculate the properties of seismic migration images to find these discontinuities. Several methods for fault identification have been proposed in previous investigations, including similarity [2], coherence [2], variance [4], and curvature [5]. In the application of complex geological tectonic zones, however, the accuracy and dependability of these methods are still problematic.

With the continuous development of artificial intelligence, deep learning is becoming increasingly popular among geophysicists [6]. The techniques of deep learning for computer vision have delivered very good results in identifying subsurface geological phenomena, such as seismic facies [7], [8], [9], [10], [11], seismic faults [12], [13], [14], [15], and salt bodies [16], [17], [18]. Convolutional neural networks (CNNs) are the most frequently used networks in computer vision. CNNs utilize multiple convolution operators as “kernels” to extract useful “features” from the input images. The kernel is presented by a matrix or tensor, which is convolved with the input image. Thus, it performs as a filter to enhance a certain desirable feature in the output image. By repeatedly using the convolution kernels in the input image, CNNs are capable of discovering features at arbitrary locations in the image [19].

Fault detection is commonly considered as a semantic segmentation problem by many researchers [20], [21]. Semantic segmentation classifies an image at the pixel level: the pixels in each sample belonging to a fault are classified as the fault class; the rest pixels are classified as the nonfault class. The network produces a probability map with the same size as the input image. The value of each pixel in the probability map shows the likelihood of the pixel being associated with a fault. As semantic segmentation-based neural networks understand images at the pixel level, they utilize the information provided in the image more effectively than classification methods [22], [23].

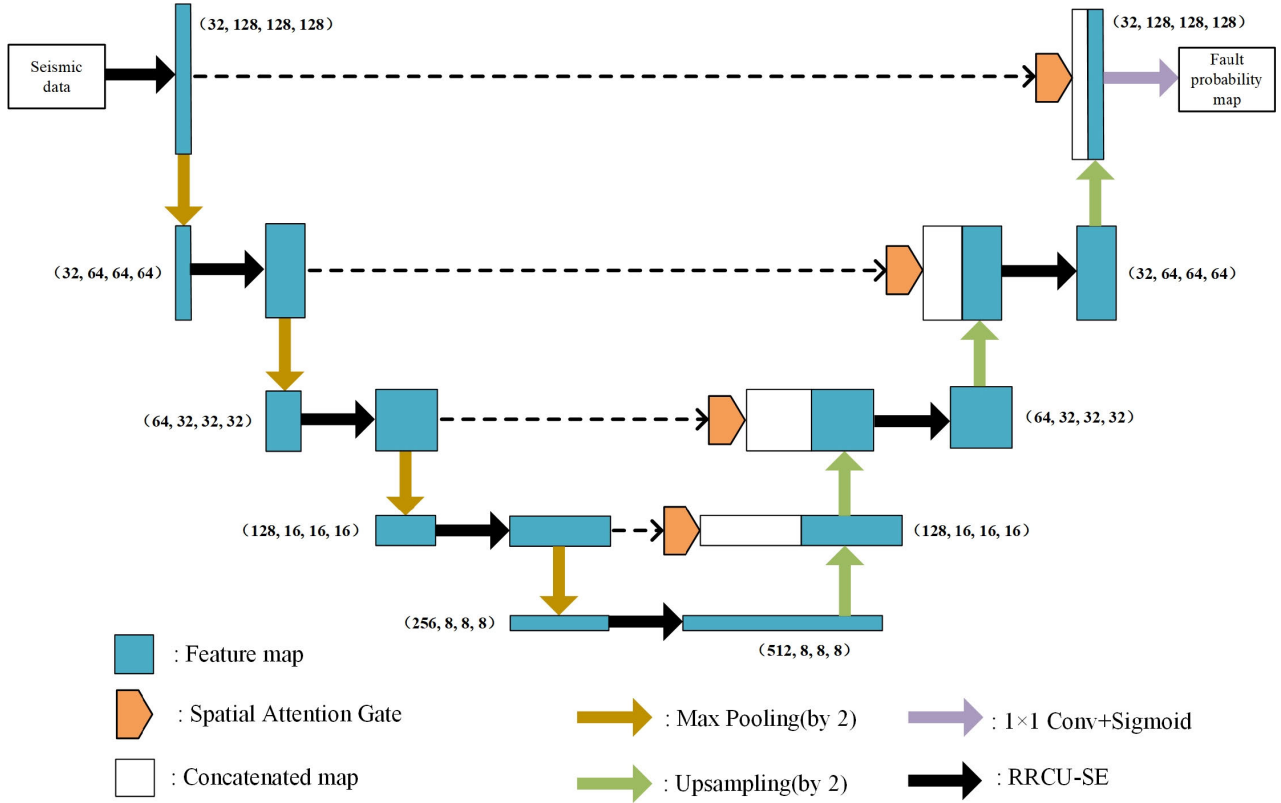


Fig. 1. Architecture of our R2SE-Unet. The input image of the network is 3-D synthetic seismic data, and the last layer of our network outputs a fault probability map with a value ranging from 0 to 1. The black arrows represent the RRCU-SE units. The purple arrow represents the combined operation of a convolutional layer with 1×1 kernel size and the Sigmoid activation function. The tuple (C, D, H, W) represents a set of feature maps, where C denotes a number of channels in the feature maps, and the dimension of the feature map is $D \times H \times W$. The upsampling layers in our R2SE-Unet use the nearest interpolation.

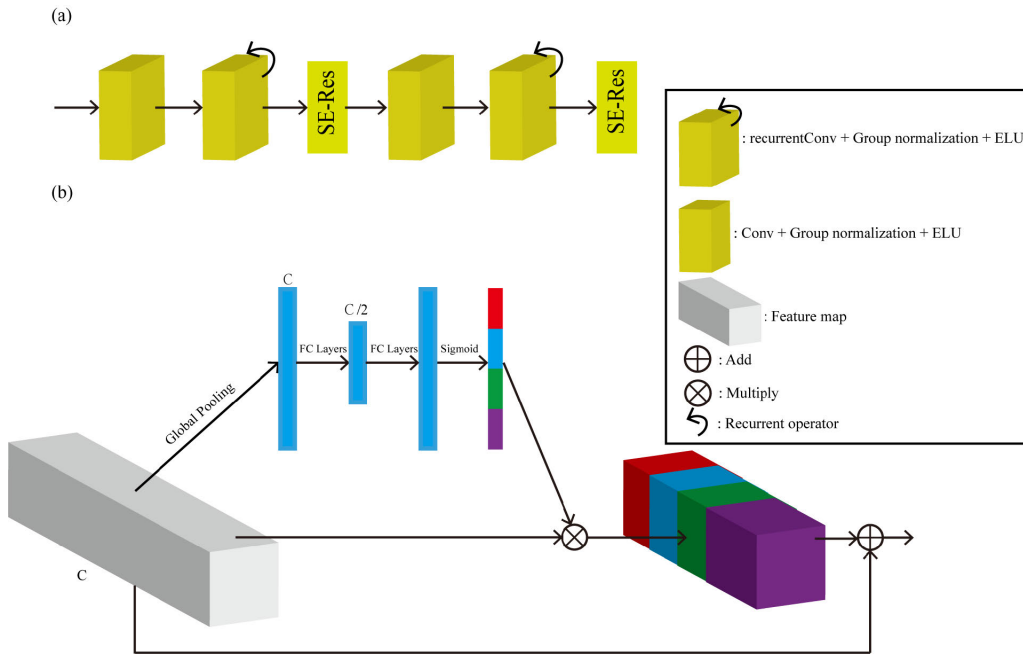


Fig. 2. Architecture of the: (a) RRCU-SE unit and (b) SE-Res block. Note that every yellow cuboid contains a convolutional layer, group normalization, and an ELU, while the white cuboid represents the feature map with C channels generated by the yellow cuboid. As shown in (a), the efficient feature accumulation operator is included in the RRCU-SE units.

Currently, the U-net network proposed by Ronneberger et al. [24] is widely used in the fault segmentation problem. The

U-net architecture includes an encoding-decoding architecture and a skip connection operation. In the encoding process, the

U-net compresses the features of the input image. In the decoding process, the U-net progressively upsamples the compressed feature maps to the shape of the input training data. U-net uses the skip connection mechanism to fuse the feature maps in the downsampling process with those in the upsampling process, which effectively mitigates the information loss caused by downsampling. Therefore, U-net performs well in various semantic segmentation applications.

In the field of geophysics, Wu et al. [25], [26] trained U-net using 3-D synthetic seismic data and tested it on 3-D field seismic data. The test results show that the U-net outperformed the traditional fault identification methods on both synthetic and field seismic data, thus demonstrating the great capability of the U-net for the fault identification problem. Some scholars modified the original U-net to achieve even better results. For instance, Gao et al. [27], [28] added a multiscale attention module to the original U-net architecture, thus resulting in more continuous fault prediction.

The loss functions also play a crucial role in the training process. In general, loss functions are classified into two types: region-based loss and distribution-based loss. Distribution-based loss, such as focal loss [29], aims to minimize dissimilarity between the predicted output and the label. Region-based loss, such as dice loss [30], aims to maximize the overlap regions between the predicted output and the label. Methods that focus on other technologies are also proposed in recent works [31], [32], [33].

We believe that two important issues constrain the effectiveness of using deep learning methods for fault detection. First, the fault systems in the field seismic data are very complex; thus, U-net does not completely distinguish a fault and its adjacent ones. This phenomenon may be caused by the structure of the convolutional units inside the U-net and the raw skip connection mechanism used in most U-net-based networks. That is, the convolutional units consisting of simple convolution operations may be inefficient for fault detection, and the raw skip connection likely causes the U-net vulnerable to noise. Second, fault detection is a problem with a highly unbalanced number of positive and negative points. That is, the “nonfault” class has much more 3-D points than the “fault” class, which is typically of the most interest. The abundance of 3-D points from the “nonfault” can overwhelm the “fault” class. Most deep learning algorithms for semantic segmentation models, including our R2SE-Unet, are designed on the assumption that classes are distributed equally. This means that most of the deep learning algorithms may only concentrate on learning the characteristics of the “nonfault” class, neglecting the samples from the “fault” class. Thus, it is crucial to design a misfit function to mitigate the imbalance problem.

To solve the two issues mentioned above, we design a new network named R2SE-Unet, which uses the architecture of recurrent neural networks (RNNs) and squeeze-excitation architecture. R2SE-Unet is inspired by medical segmentation tasks such as lung segmentation [34], [35] and brain tumor segmentation [36], [37]. Yet, we consolidate crucial modifications and improvements for seismic fault detection tasks. In more detail, we consider that the RNNs achieved

good results in natural language processing tasks because their looping operation allows the network to remember the information more effectively [38]. We take the advantage of this operation by combining RNNs with CNNs to make the model remember “where” is the most essential characteristic of faults. In addition, we use the squeeze-and-excitation residual (SE-Res) module in the convolution units to enhance the neural network’s capability to focus on the channels where the information of faults lies. We then add attention units between the feature maps during the concatenation operations. The attention units can add weight to each pixel in the feature map, thus allowing the network to focus more on the pixels belonging to the fault. We also notice that most researchers use only distribution-based loss functions or region-based loss functions as the loss function. In this article, we propose a type of loss function named generalized dice balanced binary cross entropy (GDice-bce) that combines the region-based loss function and the distribution-based loss functions. Applications on both synthetic and field data demonstrate that our R2SE-Unet trained by GDice-bce can achieve excellent results.

The rest of this article is structured as follows. We outline the R2SE-Unet architecture for fault segmentation in Section II. Then, in Section III, in order to demonstrate the advantages of our network, we compare it against two other conventional U-Net architectures using a variety of synthetic and field seismic data. In Section V, we conclude our investigation.

II. METHODOLOGY

We regard 3-D seismic fault detection problem as an image segmentation task and propose a novel convolutional network called R2SE-Unet that combines the RNN with CNN. The distribution-based loss functions, such as balanced binary cross entropy (b-BCE) loss, could produce less noise but low-probability fault feature maps while the region-based loss functions, such as GDice loss, could produce high-probability fault feature maps but are sensitive to noise. Therefore, we combine them to form a compound loss, named GDice-bce loss, to improve the performance of our R2SE-Unet.

A. Architecture

U-net is a popular network for fault detection tasks [39], [40]. It provides substantial benefits for segmentation problems: first, the network combines the information from different spatial parts of the feature maps using concatenate operation; this operation allows it to precisely localize the regions of interest and receive useful information. Second, it can learn features using few labeled images, which is well-suited for our experiment considering the sparsity of the training data. However, as noted in the “Introduction,” U-net is vulnerable to seismic noise and the fault prediction results in field seismic data can be discontinuous. To improve the antinoise performance and accuracy of fault prediction results on seismic images, we design an advanced deep learning architecture named R2SE-Unet. The architecture of our R2SE-Unet is displayed in Fig. 1, which is different from the conventional U-net.

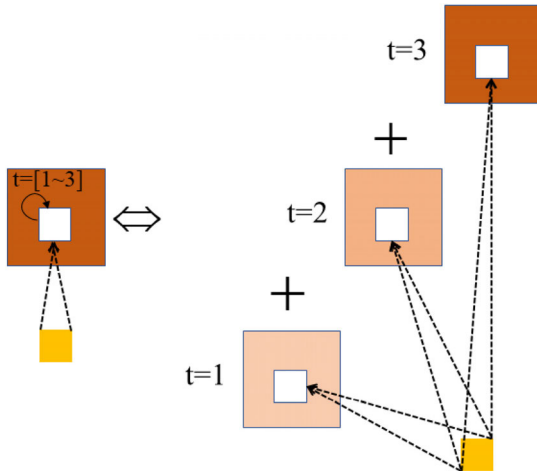


Fig. 3. Schematic of the unfolded recurrent convolution layer. The yellow rectangle represents the convolutional layer. Here, $t = [1, 2]$ represents the recurrent convolutional operation that consists of one single convolution layer followed by two subsequent recurrent convolutional layers.

In U-net, each unit in the encoder branch and decoder branch is a simple double convolution. Instead, our R2SE-Unet contains an advanced unit called recurrent residual-SE convolutional unit (RRCU-SE) to take the advantage of the RNN, which has successful applications in the modeling of sequential data, such as speech recognition. In addition, we add spatial attention gates during the concatenation operation. These gates produce a spatial attention map by exploiting the interspatial relationship of features, making our R2SE-Unet learn and concentrate more on the important information, rather than learning nonuseful background information.

The architecture of RRCU-SE is displayed in Fig. 2(a). It consists of three modules. This first module is represented by the yellow cuboids, which contains a convolutional layer, a group normalization layer, and an exponential linear unit (ELU). The second module is represented by the yellow cuboids with a circular arrow. Compared to the first module, it uses a recurrent convolutional layer instead. The third module is the SE-Res module.

The recurrent convolutional layer in the second module helps extract context information, which are crucial for fault segmentation tasks considering faults exhibit discontinuities in seismic profiles. More specifically, as shown in Fig. 3, the recurrent convolution layer enables every kernel to incorporate context information in an arbitrarily large region in the current layer. The accumulation of context information in relation to different time steps ensures richer and stronger feature representation. This recurrent operation is also regarded as a data augmentation technique [41].

It is noteworthy that we use group normalization instead of batch normalization in the RRCU-SE unit because batch normalization is not very effective if the batch size is too small. Unfortunately, due to the limitation of GPU memory size for 3-D fault images, we set the batch size to 2. Group normalization does not exploit the batch dimension, and its computation is independent of batch sizes.

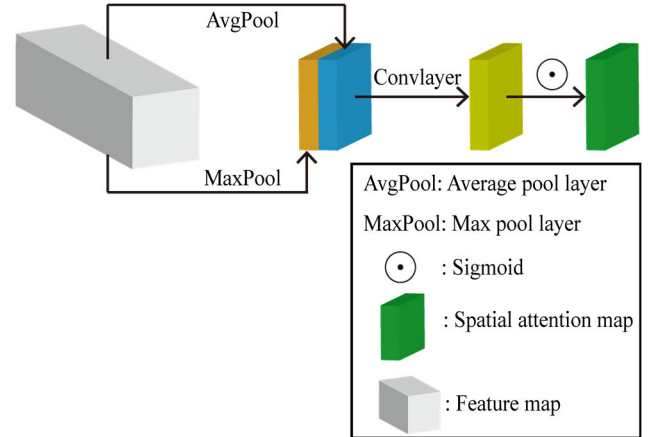


Fig. 4. Architecture of the spatial attention gate. The input feature map is decomposed into two channels, where each of the channels refers to max-pooling and average pooling. A convolution layer is then added to output a one-channel feature map. Then, the Sigmoid activation function will weigh all the values to a range between 0 and 1.

TABLE I
COMPUTATIONAL COST OF THREE NEURAL NETWORKS

Models	U-net	R2-Unet	R2SE-Unet
Total GPU memory (MB)	27846	22983	24983
Trainable weights	9739674	7152630	7261547
Training time (min)	11.4	8.7	9

With minimal computational expense, SE-Res which is depicted in Fig. 2(b) enhances nonlinear interdependencies and channel interactions between the channels. By adding a global pooling layer, the SE-Res module squeezes each channel in the feature maps to a single numeric value to get a global understanding. This operation results in a vector of size C , where C represents the number of convolution channels. A second fully connected layer followed by a Sigmoid activation outputs a vector that can be used as weights on the original feature maps. At last, we weigh each feature map based on the side network to improve the representational power of our R2SE-Unet. SE-Res also utilizes the characteristics of the deep residual model to overcome the overfitting problem [42], [43] and efficiently backpropagates the gradient information throughout the network.

In addition to the RRCU-SE unit, we also propose a spatial-attention gate using the network architecture displayed in Fig. 4. Unlike the channel attention gate, the spatial attention gate directs the model to focus on relevant regions while suppressing feature activation in unrelated regions of the feature maps. We accumulate channel information of a feature map by using two pooling processes, i.e., average pooling operation and max pooling operation, generating two feature maps, i.e., average-pooled features and max-pooled features. Then, these two feature maps are concatenated and convolved by a conventional convolution layer, generating the spatial attention map. The representational capability of the neural

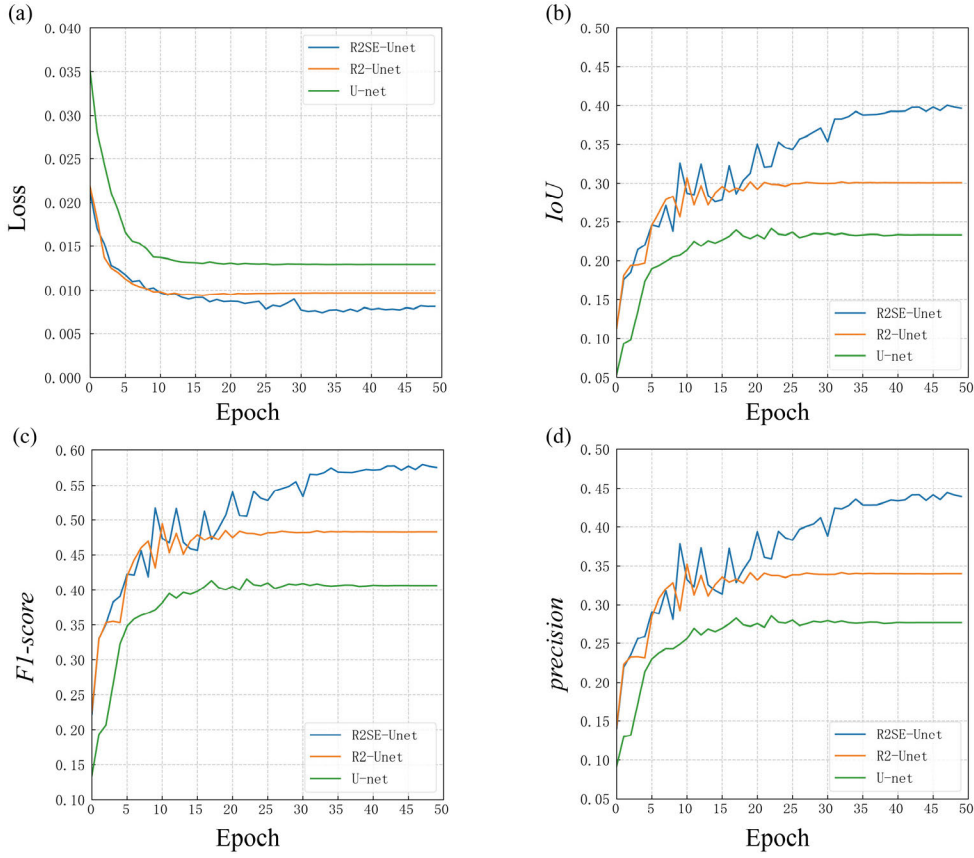


Fig. 5. (a) Validation loss curves. (b) IoU. (c) F1-score. (d) Precision. The blue, yellow, and green curves represent R2SE-Unet, R2-Unet, and U-net, respectively.

network is significantly improved by the spatial attention gate without significantly raising the cost of computing.

Overall, the R2SE-Unet has an encoder branch and a decoder branch. The encoder consists of the RRCU-SE and the max-pooling layer followed by $1 \times 1 \times 1$ convolution. The decoders consist of the RRCU-SE and the concatenation operation which combines the feature maps from the encoders. The parameter size of each encoder in R2SE-Unet is 0.055, 0.324, 0.9, and 3.6 M, respectively. The parameter size of each decoder in R2SE-Unet is 1.8, 0.552, 0.11, and 352 M, respectively. Although our R2SE-Unet architecture seems complex, it only contains approximately 7.2-M learnable weights, whereas U-net contains approximately 9.7-M learnable weights.

B. Loss Function

An appropriate loss function is important for fault detection. After many experiments, we mix the GDice loss function [44] and the b-BCE loss function [45] to form the compound loss function, GDice-bce. These loss functions are defined as

$$\begin{aligned} \mathcal{L}_{\text{b-BCE}} = & -\beta \sum_{i=1}^N \hat{y}_i \log(y_i) \\ & - (1 - \beta) \sum_{i=1}^N (1 - \hat{y}_i) \log(1 - y_i) \quad (1) \end{aligned}$$

$$\mathcal{L}_{\text{GDice}} = 1 - \frac{\omega \sum_{i=1}^N \hat{y}_i y_i}{\sum_{i=1}^N (\hat{y}_i + y_i)} \quad (2)$$

$$\hat{y}_i = \begin{cases} 1, & \text{fault} \\ 0, & \text{else} \end{cases} \quad (3)$$

$$\mathcal{L}_{\text{GDice-bce}} = \mathcal{L}_{\text{b-BCE}} + \mathcal{L}_{\text{GDice}} \quad (4)$$

where $y_i = \text{sigmoid}(x_i)$, x_i is the input of the network, \hat{y}_i is the label of the pixel, β denotes the ratio between the nonfault pixels and the total pixels, and N denotes the number of pixels in the input 3-D seismic image. b-BCE loss works well in fault segmentation tasks, but this function yields low-probability fault feature maps, which hinder the accuracy of interpretation. As for the region-based loss function, in (2), we use GDice loss to alleviate the problem of sample imbalance in fault segmentation tasks. More specifically, we set $\omega = 1/(\sum_{i=1}^N \hat{y}_i)^2$ to mitigate the high imbalance in our experiment. It should be noted that there are other definitions for the GDice loss function, and the one we proposed is appropriate for our fault detection experiment. In our experiment, GDice could yield high-probability fault feature maps but is vulnerable to noise. Through extensive numerical tests, as shown in (4), we find that the combination of the GDice loss and b-BCE loss could produce stable segmentation results with better antinoise performance.

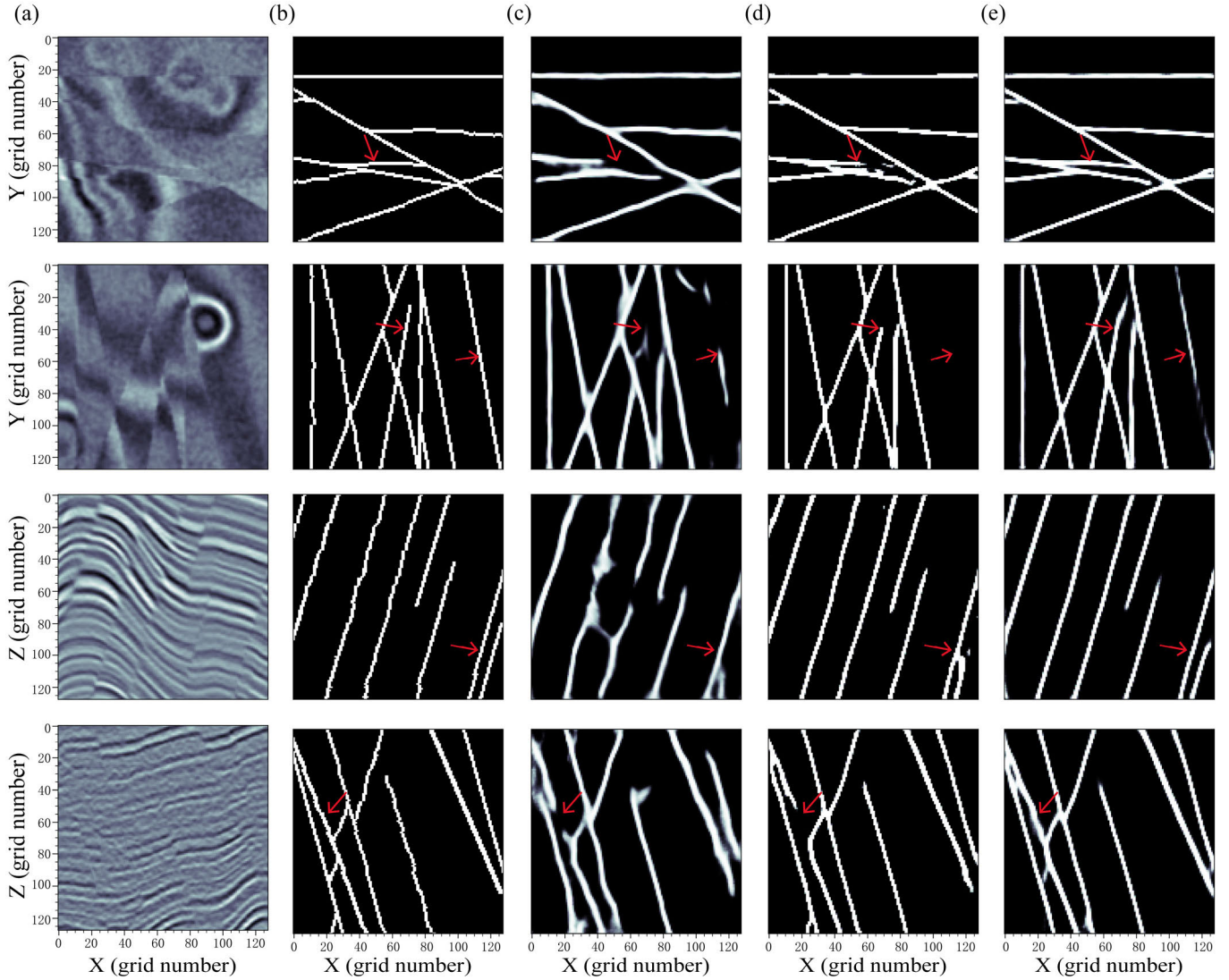


Fig. 6. Fault detection on the synthetic validation volume: (a) represents the synthetic images; (b) represents the corresponding labels; and (c)–(e) represent the faults detected using U-net, R2-Unet, and R2SE-Unet, respectively.

C. Accuracy Measurement

We use the following accuracy measurements to assess the performance of the trained network.

1) Intersection over union (IoU)

$$\text{IoU} = \frac{n_{\text{TP}}}{n_{\text{FP}} + n_{\text{TP}} + n_{\text{FN}}}. \quad (5)$$

2) Precision

$$\text{precision} = \frac{n_{\text{TP}}}{n_{\text{TP}} + n_{\text{FP}}}. \quad (6)$$

3) F1-score

$$\text{sensitivity} = \frac{n_{\text{TP}}}{n_{\text{TP}} + n_{\text{FN}}} \quad (7)$$

$$\text{F1-score} = \frac{2 \cdot \text{precision} \cdot \text{sensitivity}}{\text{precision} + \text{sensitivity}}. \quad (8)$$

Here,

$$n_{\text{TP}} = \sum_{i=1}^N (\text{label} = 1) \&\& (\text{prediction} = 1)$$

$$n_{\text{TN}} = \sum_{i=1}^N (\text{label} = 0) \&\& (\text{prediction} = 0)$$

$$n_{\text{FP}} = \sum_{i=1}^N (\text{label} = 0) \&\& (\text{prediction} = 1)$$

$$n_{\text{FN}} = \sum_{i=1}^N (\text{label} = 1) \&\& (\text{prediction} = 0) \quad (9)$$

where “ $\&\&$ ” denotes the logical operation “AND.” According to the definitions, precision indicates how many of the pixels predicted by the network as faults are correct, and sensitivity represents the percentage of the fault pixels that are correctly predicted by the network and measures the network’s ability to identify the faults. F1-score combines accuracy and specificity. As a result, a higher F1-score indicates that the network predicts a lot of positive pixels and ensures that a high percentage of the predicted positive pixels is correct.

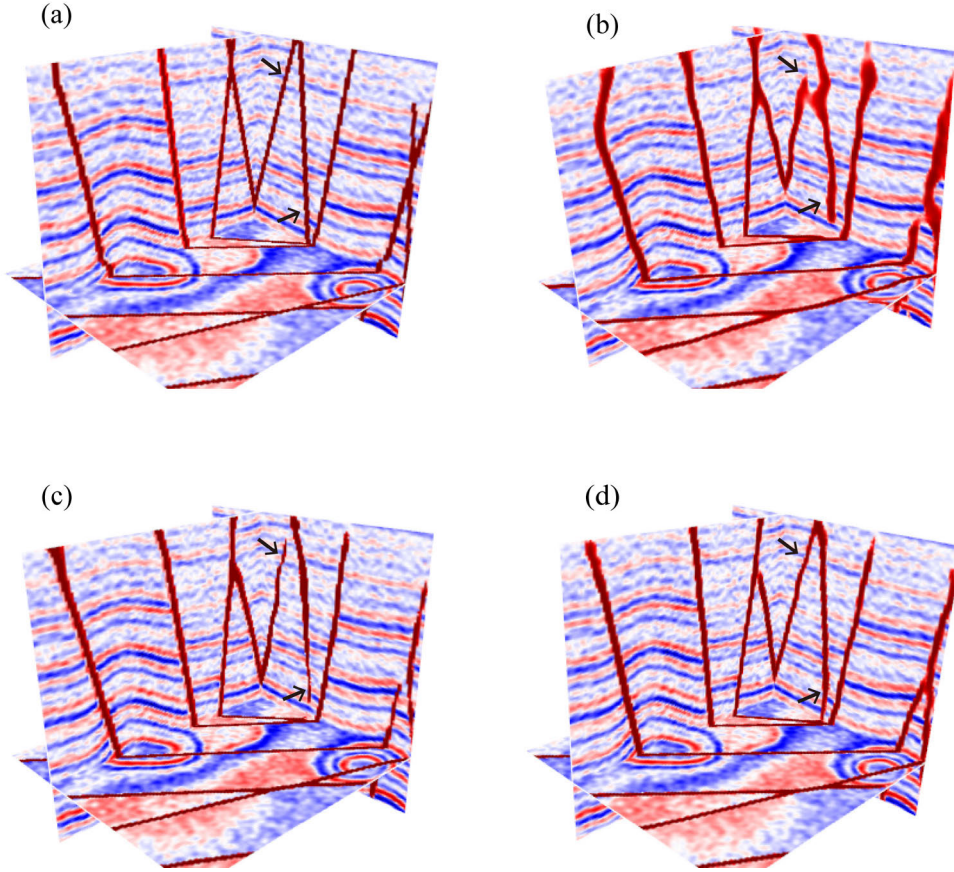


Fig. 7. (a) Synthetic seismic data and ground truth. (b)–(d) Represent the fault detection result of U-net, R2-Unet, and R2SE-Unet, respectively.

D. Data Preparation and Training Settings

In our training process, we use only synthetic seismic data and corresponding labels to train the R2SE-Unet. We generate the training data that contain multiple types of faults using the method proposed by Wu et al. [26]. We randomly generate 800 pairs of synthetic 3-D seismic images and 100 pairs of 3-D images as the validation dataset for the R2SE-Unet. To prevent ambivalence due to the seismic amplitude variations across different datasets, both synthetic seismic data and field seismic data are normalized: subtracted by the mean value and then divided by the standard deviation value.

We deploy R2SE-Unet in PyTorch Lightning, which is a PyTorch-based deep learning framework with maximal flexibility. We train networks using two RTX 3090 GPUs. We use the Adam optimizer [46] to update the parameters inside the neural network, and the initial learning rate we used is 0.0008. A large learning rate typically enables the model to learn more quickly at the expense of producing a suboptimal final set of weights. By contrary, a small learning rate has a tendency to produce weights that are globally optimal, but the training process may take much longer. To overcome this problem, we presume that the learning algorithm can keep track of the model's performance on the training dataset and modify the learning rate accordingly. In other words, when the validation accuracy appears to plateau, then the learning rate will be reduced by a factor of 0.5.

We implement two different Unet-based networks in order to evaluate the effectiveness of our R2SE-Unet for fault detection. The first neural network is the conventional U-net presented by Wu et al. [26]. This neural network is known as U-net. The second neural network is the same R2SE-Unet except that we remove the SE-Res module in every unit. We denote this architecture as R2-Unet. We train and validate these two networks using the same synthetic datasets for R2SE-Unet. The loss function we used in this experiment is our GDice-bce loss function. In addition, the computational cost of these three models is listed in Table I. Fig. 5 displays the loss and metrics curves of the validation phase. The metrics indicate that our R2SE-Unet performs better than the other two models. We also observe that our R2SE-Unet has higher noise resistance and can predict more faults in field seismic data tests. More details about the performance are described in Section III.

III. APPLICATIONS

In this section, we test the generalization ability and performance stability of our network and loss function on the seismic images of one synthetic dataset and two field datasets. The datasets used in this section are directly fed to the networks after standardization. Despite the model being trained using only synthetic datasets, it has outstanding performance on both synthetic and field seismic data.

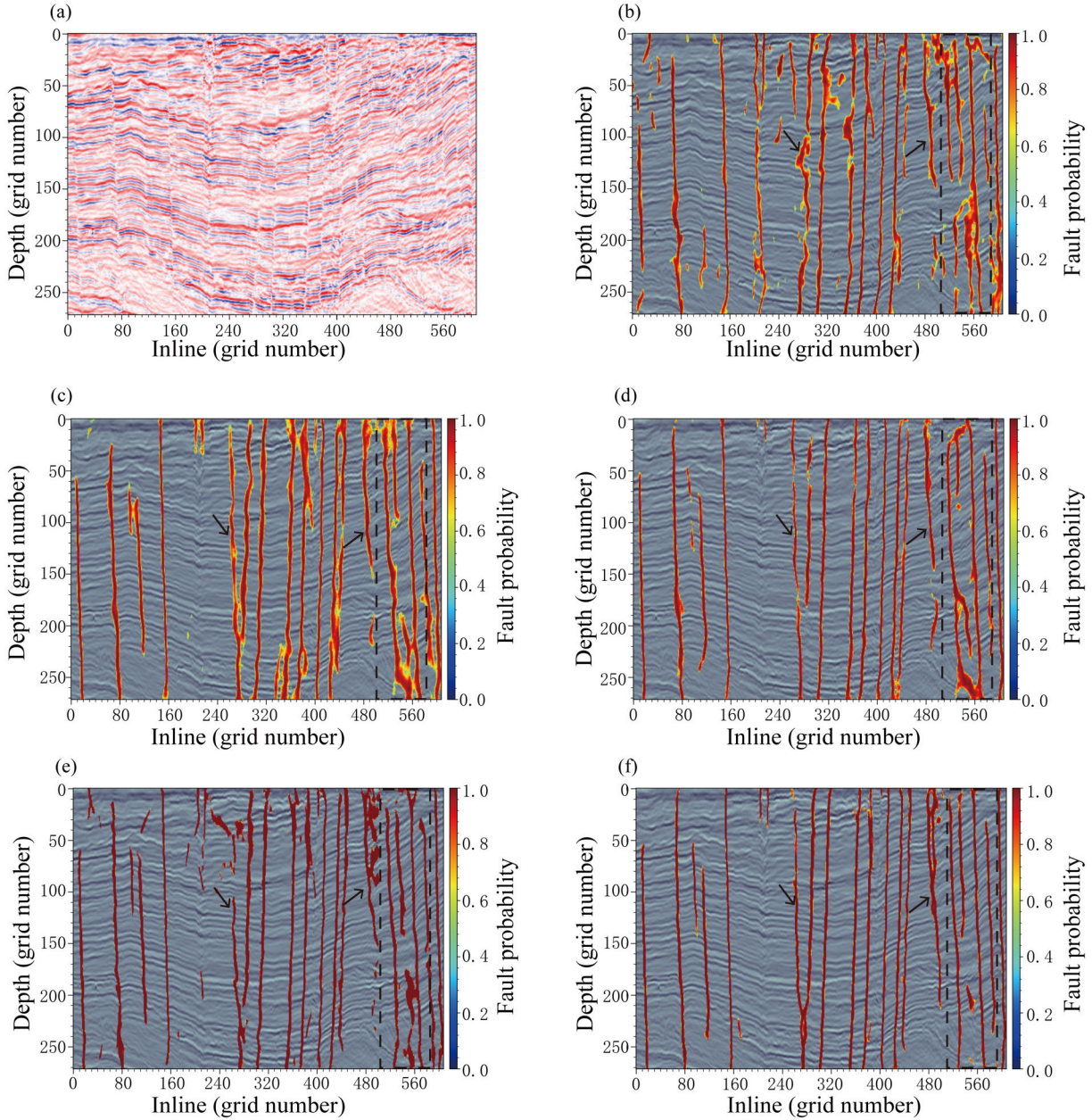


Fig. 8. (a) Slice of Kerry seismic data is overlaid with faults detected by using: (b) U-net + b-BCE; (c) R2-Unet + b-BCE; (d) R2SE-Unet + b-BCE; (e) R2SE-Unet + GDice; and (f) R2SE-Unet + GDice-bce.

A. Synthetic Seismic Data

The comparison among U-net, R2-Unet, and our R2SE-Unet for the 3-D synthetic seismic data is shown in Fig. 6. The first column displays the synthetic seismic images, the second column shows the ground-truth fault probability maps, and the third–fifth columns show the faults prediction results using U-net, R2-Unet, and our R2SE-Unet, respectively. Despite the U-net and R2-Unet can predict many faults, these two models miss minor faults or make incorrect fault prediction, especially when several faults are clustered. For example, on the third image, the red arrow indicates that these two faults are close to each other, and U-net and R2-Unet produce erroneous predictions in this area. In contrast, our R2SE-Unet detects these faults precisely.

To better visualize the advancement of our R2SE-Unet compared with the U-net and R2-Unet, Fig. 7 shows one synthetic seismic image from the validation dataset in a 3-D view. It is obvious that U-net has a very ambiguous prediction, and R2-Unet gives a low-continuity prediction. In contrast, the R2SE-Unet produces a much better prediction in terms of resolution and continuity than the other two models, thus demonstrating its superior performance.

Then, we demonstrate the superiority of R2SE-Unet and the proposed loss functions on field data. In the experiment of different field data, we find that R2SE-Unet trained by the compound loss function could produce more geological interpretable faults than other networks trained by a single loss function. To demonstrate this finding, in the following examples, we use different combinations of networks and loss

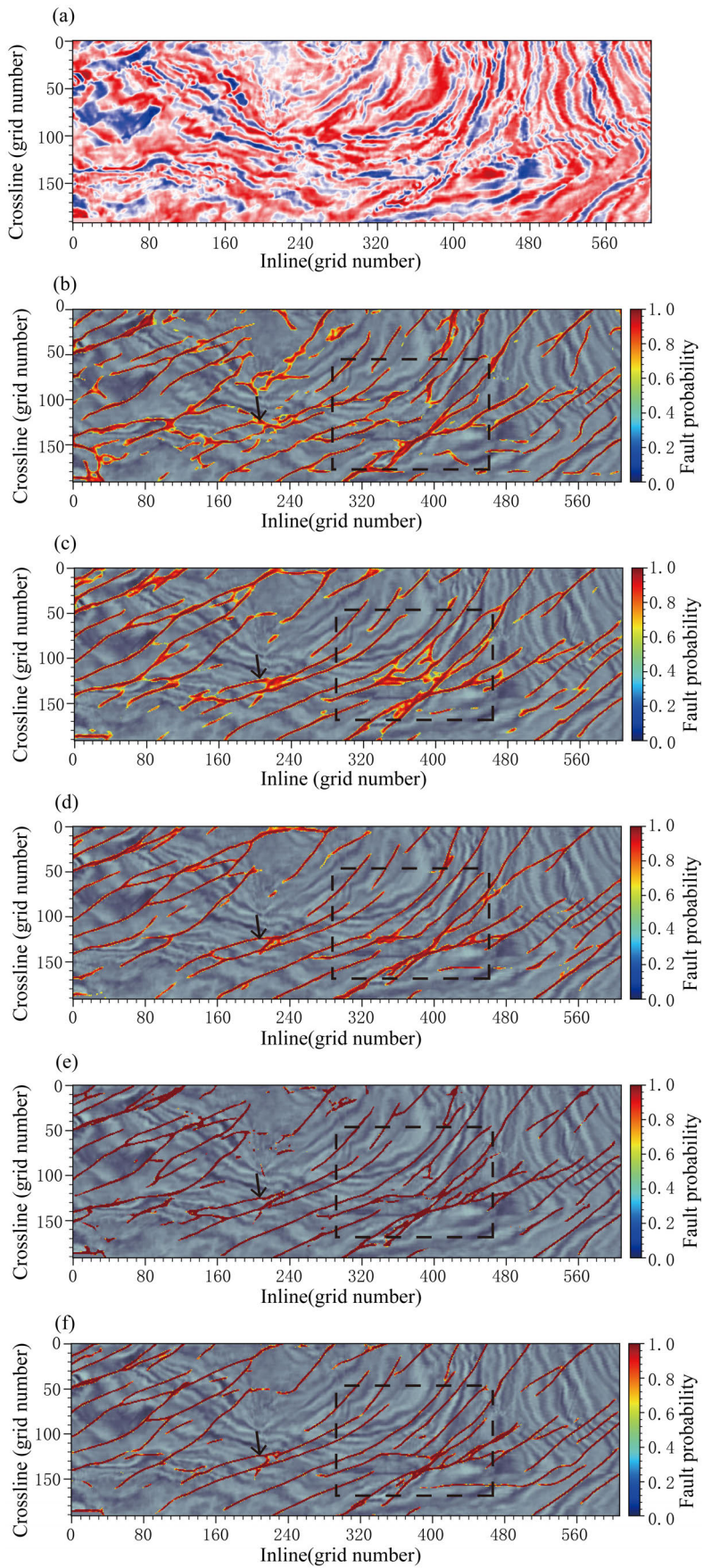


Fig. 9. (a) Horizontal slice of Kerry seismic data is overlaid with faults detected by using: (b) U-net + b-BCE; (c) R2-Unet + b-BCE; (d) R2SE-Unet + b-BCE; (e) R2SE-Unet + GDice; and (f) R2SE-Unet + GDice-bce.

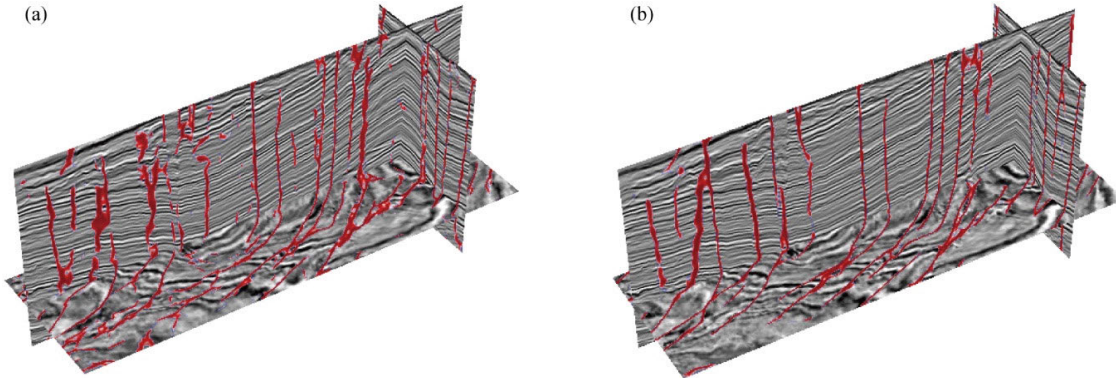


Fig. 10. Subset of Kerry seismic data wrapped by the fault prediction results using: (a) U-net + b-BCE and (b) our R2SE-Unet + b-BCE.

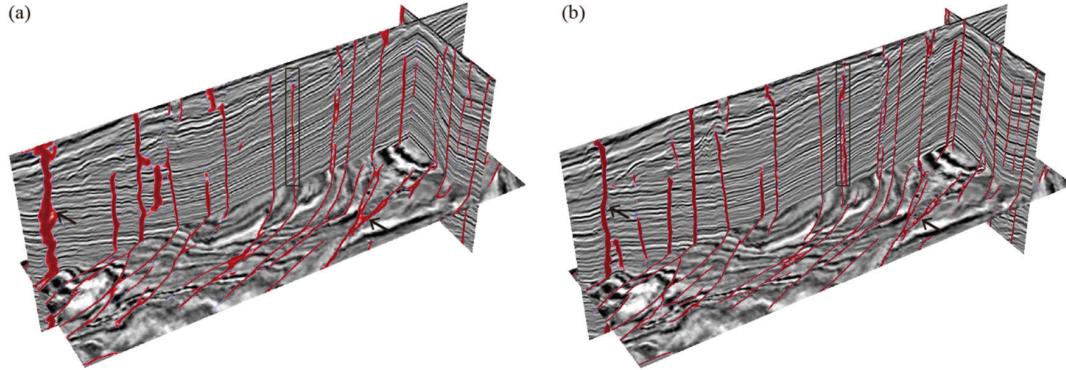


Fig. 11. Subset of Kerry seismic data wrapped by the fault prediction results using: (a) R2SE-Unet + b-BCE and (b) R2SE-Unet + GDice-bce.

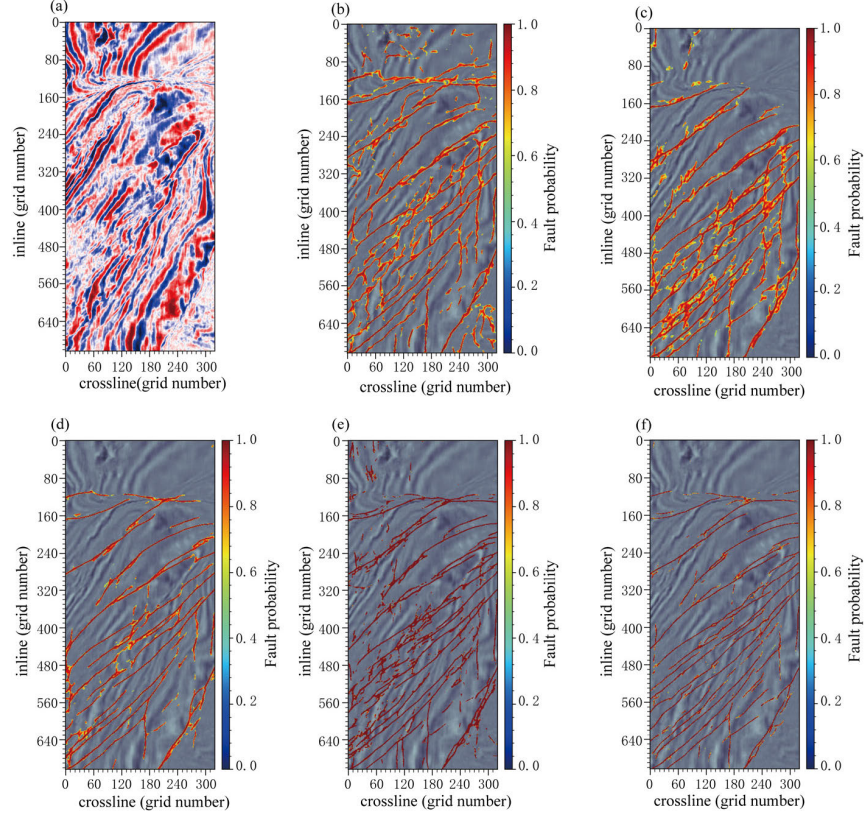


Fig. 12. (a) Horizontal slice of Opunake seismic data is overlaid with faults detected by using: (b) U-net + b-BCE; (c) R2-Unet + b-BCE; (d) R2SE-Unet + b-BCE; (e) R2SE-Unet + GDice; and (f) R2SE-Unet + GDice-bce.

functions to compare with the combination of our R2SE-Unet network and GDice-bce loss function. The “network +

loss function” in the captions of Figs. 8–15 represents the “network” trained by the “loss function.”

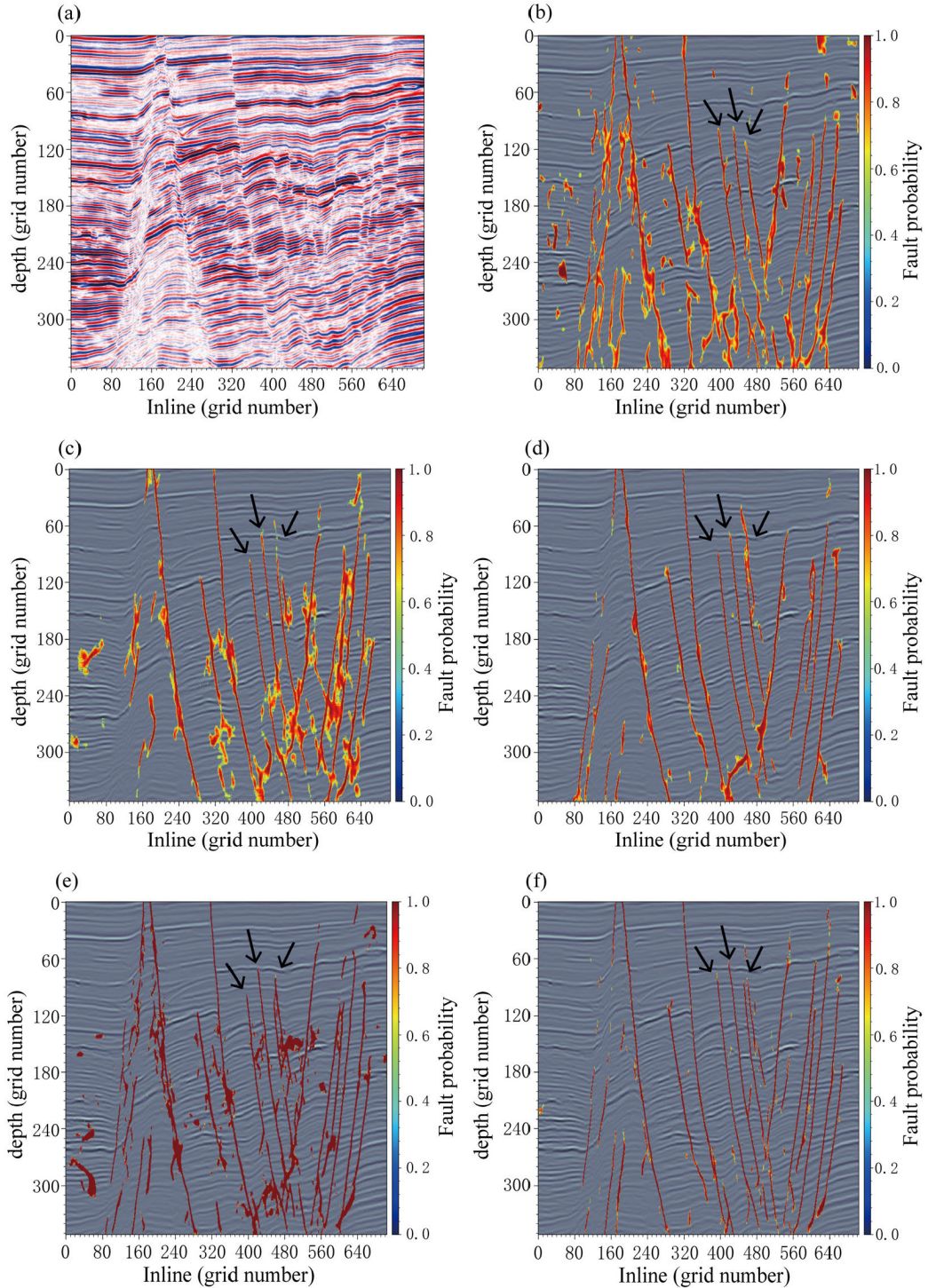


Fig. 13. (a) Slice of Opunake seismic data is overlaid with faults detected by using: (b) U-net + b-BCE; (c) R2-Unet + b-BCE; (d) R2SE-Unet + b-BCE; (e) R2SE-Unet + GDice; and (f) R2SE-Unet + GDice-bce.

B. Kerry 3-D

The first 3-D seismic dataset named Kerry 3-D is provided by the New Zealand Crown Minerals, Wellington, New Zealand. The faults of this seismic data are very close to each other and numerous, so it is difficult to detect the fault, but our proposed “R2SE-Unet + GDice-bce” method still yields a clear and accurate interpretation of the faults. Figs. 8 and 9 show the results of fault segmentation using different networks and loss functions. More specifically, as shown

in Figs. 8 and 9, “Unet + b-BCE” produces significant discontinuity faults on the 3-D slices, and this method is very susceptible to noise. In contrast, “R2SE-Unet + GDice-bce” obtains a more reliable delineated result with better anti-noise performance. The segmented faults have defined edges, isolated from the background, and no visible discontinuous faults, whether observed from inline or horizontal orientations. The background area is clean, demonstrating that our neural network can significantly reduce seismic noise jamming.

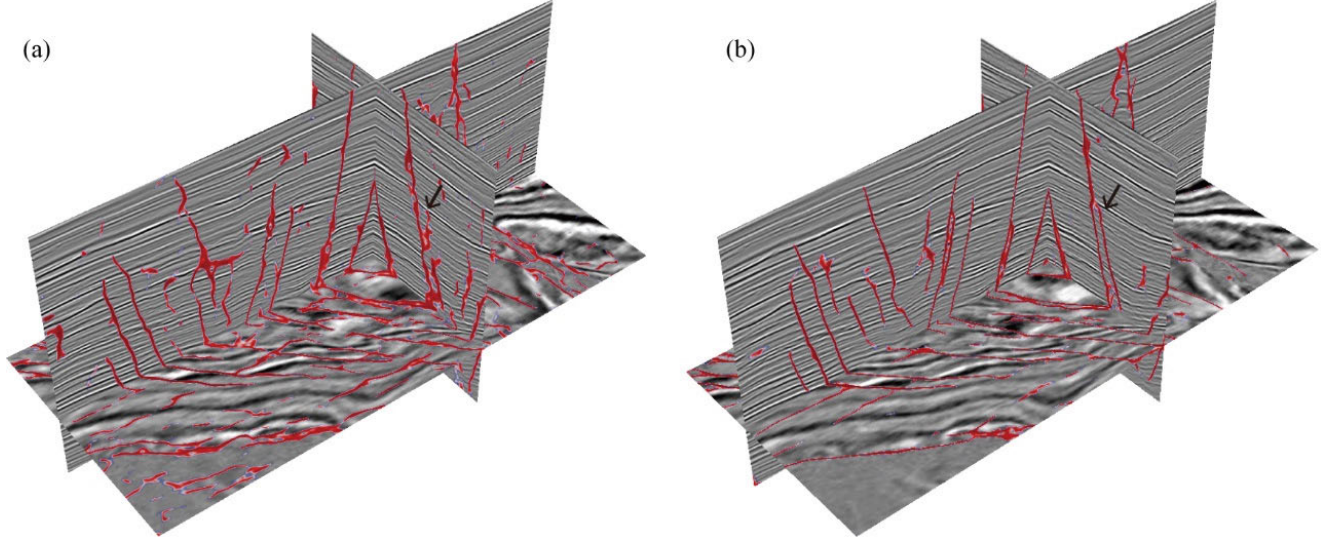


Fig. 14. Subset of Opunake seismic data wrapped by the fault prediction results using: (a) U-net + b-BCE and (b) our R2SE-Unet + b-BCE.

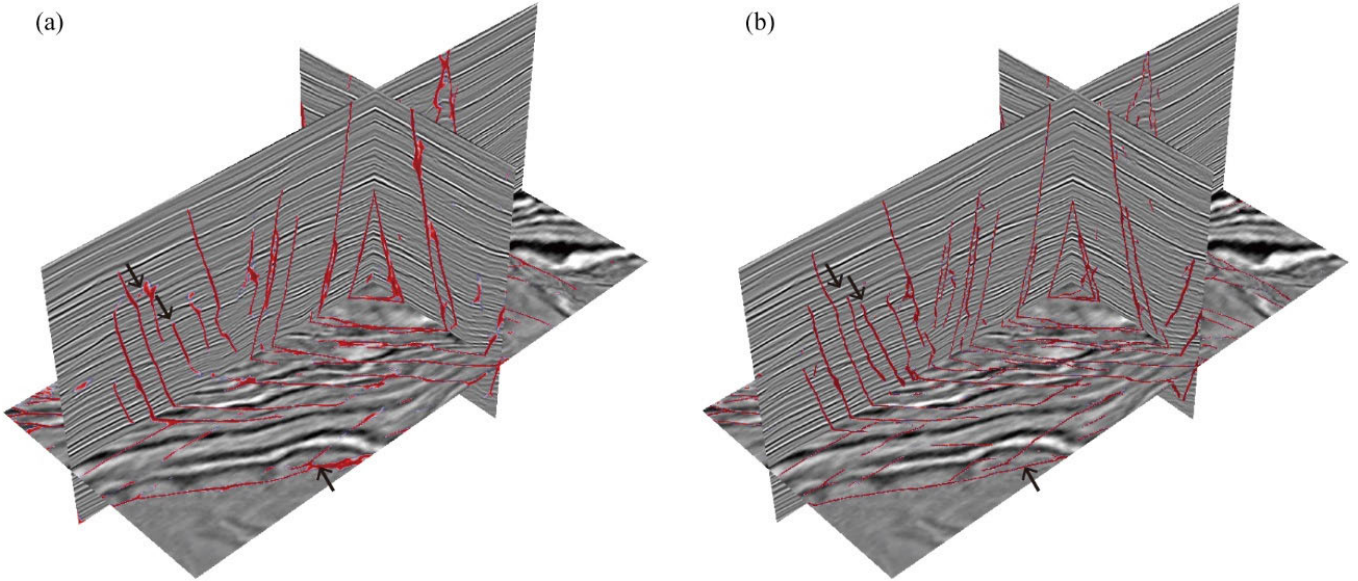


Fig. 15. Subset of Opunake seismic data wrapped by the fault prediction results using: (a) R2SE-Unet + b-BCE and (b) R2SE-Unet + GDice-bce.

Figs. 10 and 11 show the 3-D view. The black arrow in Fig. 11 indicates that the fault can be predicted by “R2SE-Unet + b-BCE” but not by “U-net + b-BCE.” In addition, the fault detection result of our “R2SE-Unet + GDice-bce” method has a high lateral resolution. Our neural network can detect and distinguish two neighboring faults even when the distance between them is very near. For example, our “R2SE-Unet + Gdice-bce” method can distinguish two very close faults in the black rectangle of Fig. 11. The edges of the faults are clear and delicate. Our method appears to be more effective at identifying faults across different directions and produces comparatively high continuity and resolution fault prediction results.

C. Opunake 3-D

In the final example, we contrast the fault detection results of the three models using Opunake-3-D, which is a field seismic dataset published at SEG Wiki. It contains a com-

plicated fault structure, which is very difficult for humans to pick manually. As shown in Figs. 12 and 13, except our “R2SE-Unet + GDice-bce,” all other methods can be overly sensitive to faults and predict many scattered and artificial faults. In contrast, our method could interpret cleaner seismic faults shown in Figs. 12(f) and 13(f).

As shown in Fig. 14, the faults predicted by using “R2SE-Unet + b-BCE” are cleaner and smoother than those interpreted by “U-net + b-BCE.” Furthermore, in Fig. 15, due to the enhanced continuity of fault lines and resolution, “R2SE-Unet + GDice-bce” could achieve the most geological interpretable fault result. We have reason to believe that the “R2SE-Unet + GDice-bce” is more effective than other networks and loss functions.

In this section, we illustrate the efficiency of R2SE-Unet and GDice-bce loss functions by comparing the fault detection results of different combinations of networks and loss functions. In multiple experiments, our “R2SE-Unet + GDice-bce”

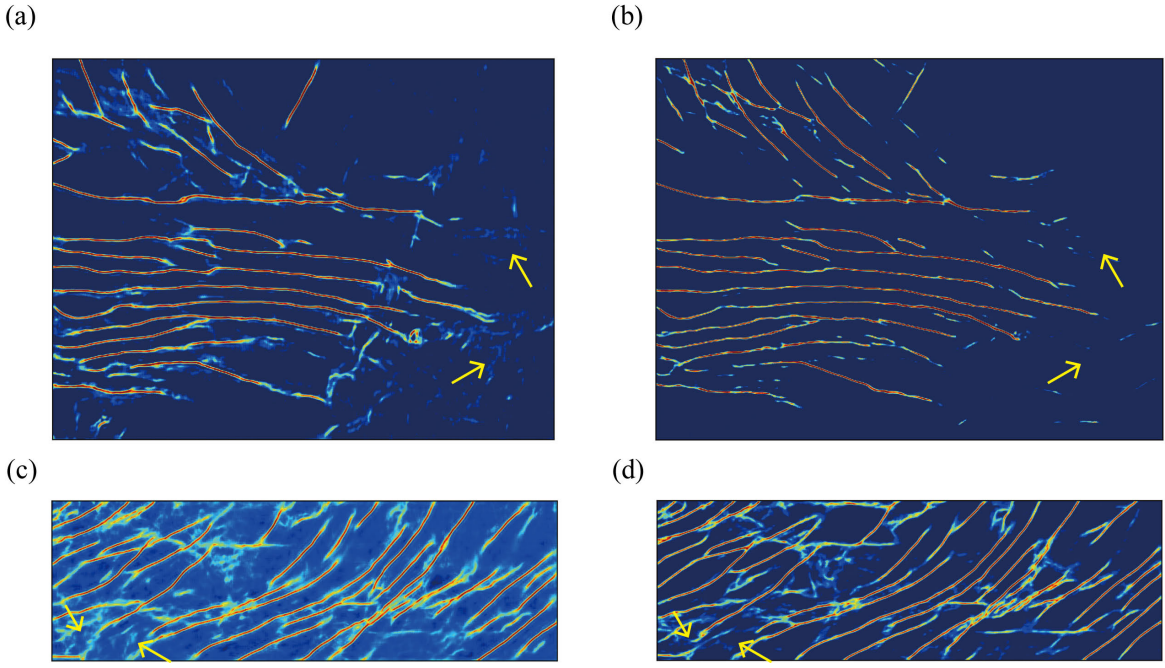


Fig. 16. Feature map of F3 seismic data predicted by: (a) CUnet and (b) R2SE-Unet; a feature map of Kerry seismic data predicted by: (c) CUnet and (d) R2SE-Unet.

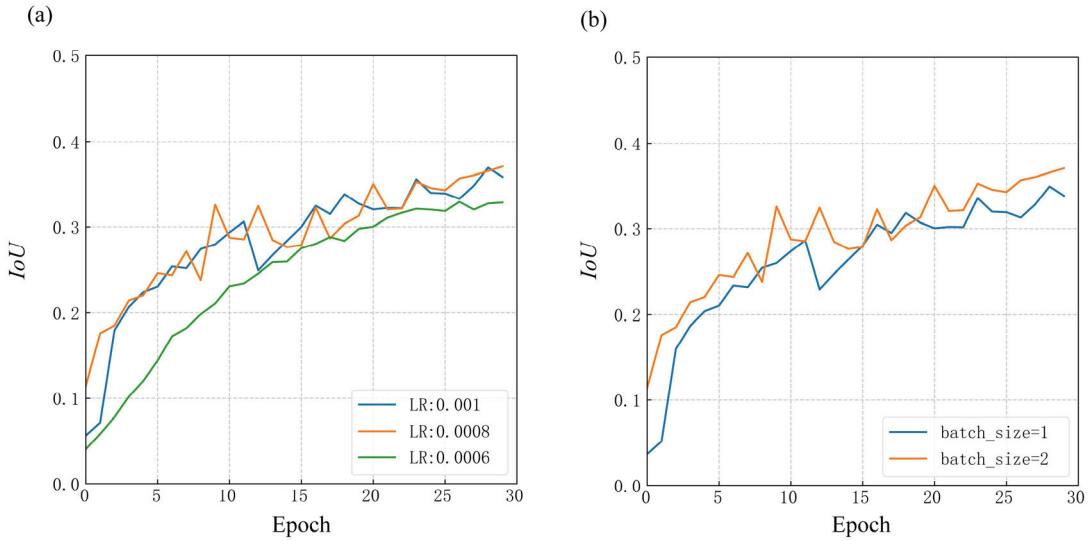


Fig. 17. Variation of IoU values with training epochs of R2SE-Unet under: (a) different learning rates and (b) batch sizes.

method can predict more continuous and higher resolution faults from both synthetic and field seismic data, especially, first, more faults identified; second, higher antinoise ability; and third, finer predicted faults.

IV. DISCUSSION

In this article, we propose a novel CNN that integrates RNN to enhance the accuracy of fault detection tasks. After a series of experiments, we list some discussions as follows.

A. RNN Versus CNN

Our tests show that our R2SE-Unet has a higher antinoise ability than R2-Unet and U-net. We presume that the recur-

rent convolutional layer can extract very low-level features via repeated convolution operators to improve the antinoise ability. To further prove the efficiency of RNN, we replace the recurrent convolutional layers of R2SE-Unet with normal convolutional layers. This model is then named as CUnet. We use field seismic data to produce feature maps of these two models. It is noteworthy that the feature maps generated in this article are extracted from the end of the decoding stage of the network. This is because in the encoding stage, the feature maps are compressed to a small size, making it difficult to distinguish the seismic faults. As shown in Fig. 16, indicated by the yellow arrow, R2SE-Unet is more noise-resistant, while CUnet produces many artifacts that are not faults.

B. Hyperparameter Setting

Hyperparameters have a significant impact on network performance. Here, as a comparison, we train the network using different learning rates and batch sizes. Fig. 17(a) clearly shows that a larger learning rate leads to significant oscillations in the IoU values during the training process, which affects the selection of the network weight files in the final testing stage. On the other hand, a smaller learning rate results in a slower convergence rate, thus leading to higher time costs. Based on the tests, we chose a learning rate of 0.0008.

Limited by the GPU memory size, i.e., 2×24 GB, we used a batch size of two. However, a smaller batch size of 1 decreases the performance of the network slightly, thus resulting in noise in the fault probability maps.

C. Limitations

One of the biggest challenges in deep learning is generalization. Although the method proposed in this article has achieved good prediction results in multiple field seismic datasets, there may still be issues with inaccurate fault prediction in some field seismic data where the fault system is more complex and the fault features are less distinct. An effective method to improve the generalization ability of the network is to enhance the diversity of the training set. In future work, we will increase the range of network learning by adding various fault types in synthetic seismic data.

V. CONCLUSION

We built a novel semantic segmentation model, named R2SE-Unet, to effectively learn the characteristics of faults. The RRCU-SE unit inside the network takes the advantage of RNNs. Feature accumulation with RRCU-SE ensures better feature representation for fault segmentation tasks. We add an attention module named SE-Res into the RRCU-SE unit, which helps R2SE-Unet to improve the antinoise ability. During the concatenation operation, we also implement the spatial-attention gates to weigh the pixels of feature maps. Moreover, we propose a compound loss function called GDice-bce loss, which combined the region-based loss and distribution-based loss. Even though we only use 3-D synthetic seismic datasets to train our network, the R2SE-Unet trained by GDice-bce can directly predict the faults in field seismic data without further training. We demonstrate the excellent fault detection capability compared with U-net and R2-Unet trained by single loss function. In the experiment of field data, we find that our R2SE-Unet trained by GDice-bce can produce a higher resolution, higher fidelity fault map with better antinoise performance. The networks and examples presented in this article can be accessed via https://github.com/wavetomo/3d_fault.

REFERENCES

- [1] Q. Gan and D. Elsworth, "Analysis of fluid injection-induced fault reactivation and seismic slip in geothermal reservoirs," *J. Geophys. Res., Solid Earth*, vol. 119, no. 4, pp. 3340–3353, Mar. 2014.
- [2] K. J. Marfurt, R. L. Kirlin, S. L. Farmer, and M. S. Bahorich, "3-D seismic attributes using a semblance-based coherency algorithm," *Geophysics*, vol. 63, no. 4, pp. 1150–1165, Jul. 1998.
- [3] K. J. Marfurt, R. L. Kirlin, S. L. Farmer, and M. S. Bahorich, "3-D seismic attributes using a semblance-based coherency algorithm," *Geophysics*, vol. 63, no. 4, pp. 1150–1165, Jul. 1998.
- [4] P. P. Van and R. E. Pepper, "Seismic signal processing method and apparatus for generating a cube of variance values," U.S. Patent 6 151 555A, Nov. 6, 2000.
- [5] T. H. Boe and R. Daber, "Seismic features and the human eye: RGB blending of azimuthal curvatures for enhancement of fault and fracture interpretation," in *Proc. SEG Tech. Program Expanded Abstr.*, Jan. 2010, pp. 1535–1539.
- [6] S. Yuan, J. Liu, S. Wang, T. Wang, and P. Shi, "Seismic waveform classification and first-break picking using convolution neural networks," *IEEE Geosci. Remote Sens. Lett.*, vol. 15, no. 2, pp. 272–276, Feb. 2018.
- [7] Y. Alaudah, P. Michalowicz, M. Alfarraj, and G. AlRegib, "A machine-learning benchmark for facies classification," *Interpretation*, vol. 7, no. 3, pp. 175–187, Aug. 2019.
- [8] F. Li, H. Zhou, Z. Wang, and X. Wu, "ADDCNN: An attention-based deep dilated convolutional neural network for seismic facies analysis with interpretable spatial-spectral maps," *IEEE Trans. Geosci. Remote Sens.*, vol. 59, no. 2, pp. 1733–1744, Feb. 2021.
- [9] R. Feng, N. Balling, D. Grana, J. S. Dramsch, and T. M. Hansen, "Bayesian convolutional neural networks for seismic facies classification," *IEEE Trans. Geosci. Remote Sens.*, vol. 59, no. 10, pp. 8933–8940, Oct. 2021.
- [10] E. Tolstaya and A. Egorov, "Deep learning for automated seismic facies classification," *Interpretation*, vol. 10, no. 2, pp. 31–40, May 2022.
- [11] S. Yuan, X. Jiao, Y. Luo, W. Sang, and S. Wang, "Double-scale supervised inversion with a data-driven forward model for low-frequency impedance recovery," *Geophysics*, vol. 87, no. 2, pp. 165–181, Mar. 2022.
- [12] A. Cunha, A. Pochet, H. Lopes, and M. Gattass, "Seismic fault detection in real data using transfer learning from a convolutional neural network pre-trained with synthetic seismic data," *Comput. Geosci.*, vol. 135, Feb. 2020, Art. no. 104344.
- [13] A. Pochet, P. H. B. Diniz, H. Lopes, and M. Gattass, "Seismic fault detection using convolutional neural networks trained on synthetic poststacked amplitude maps," *IEEE Geosci. Remote Sens. Lett.*, vol. 16, no. 3, pp. 352–356, Mar. 2019.
- [14] H. Di, Z. Wang, and G. AlRegib, "Seismic fault detection from post-stack amplitude by convolutional neural networks," in *Proc. EAGE Conf. Exhib.*, Jun. 2018, pp. 1–5.
- [15] K. Zhang, N.-T. Lin, J.-Q. Yang, Z.-W. Jin, G.-H. Li, and R.-W. Ding, "Predicting gas-bearing distribution using DNN based on multi-component seismic data: Quality evaluation using structural and fracture factors," *Petroleum Sci.*, vol. 19, no. 4, pp. 1566–1581, Aug. 2022.
- [16] Y. Shi, X. Wu, and S. Fomel, "SaltSeg: Automatic 3D salt segmentation using a deep convolutional neural network," *Interpretation*, vol. 7, no. 3, pp. E113–122, Aug. 2019.
- [17] Z. Geng, Z. Hu, X. Wu, L. Liang, and S. Fomel, "Semisupervised salt segmentation using mean teacher," *Interpretation*, vol. 10, no. 3, pp. 21–29, Aug. 2022.
- [18] S. Yuan, J. Wang, T. Liu, T. Xie, and S. Wang, "6D phase-difference attributes for wide-azimuth seismic data interpretation," *Geophysics*, vol. 85, no. 6, pp. 37–49, Nov. 2020.
- [19] Y. LeCun, K. Kavukcuoglu, and C. Farabet, "Convolutional networks and applications in vision," in *Proc. IEEE Int. Symp. Circuits Syst.*, May 2010, pp. 253–256.
- [20] L. Lin, Z. Zhong, Z. Cai, A. Y. Sun, and C. Li, "Automatic geologic fault identification from seismic data using 2.5D channel attention U-Net," *Geophysics*, vol. 87, no. 4, pp. 111–124, Jul. 2022.
- [21] S. Li, N. Liu, F. Li, J. Gao, and J. Ding, "Automatic fault delineation in 3-D seismic images with deep learning: Data augmentation or ensemble learning?" *IEEE Trans. Geosci. Remote Sens.*, vol. 60, 2022, Art. no. 5911214.
- [22] A. Guitton, "3D convolutional neural networks for fault interpretation," in *Proc. 80th EAGE Conf. Exhib.*, Jun. 2018, pp. 1–5.
- [23] K.-H. Sang, X.-Y. Yin, and F.-C. Zhang, "Machine learning seismic reservoir prediction method based on virtual sample generation," *Petroleum Sci.*, vol. 18, no. 6, pp. 1662–1674, Dec. 2021.
- [24] O. Ronneberger, P. Fischer, and T. Brox, "U-Net: Convolutional networks for biomedical image segmentation," in *Proc. Int. Conf. Med. Image Comput. Comput.-Assist. Intervent.* Cham, Switzerland: Springer, 2015, pp. 234–241.

- [25] X. Wu, L. Liang, Y. Shi, and S. Fomel, "FaultSeg3D: Using synthetic data sets to train an end-to-end convolutional neural network for 3D seismic fault segmentation," *Geophysics*, vol. 84, no. 3, pp. 35–45, May 2019.
- [26] X. Wu, Z. Geng, Y. Shi, N. Pham, S. Fomel, and G. Caumon, "Building realistic structure models to train convolutional neural networks for seismic structural interpretation," *Geophysics*, vol. 85, no. 4, pp. 27–39, Jul. 2020.
- [27] K. Gao, L. Huang, and Y. Zheng, "Fault detection on seismic structural images using a nested residual U-Net," *IEEE Trans. Geosci. Remote Sens.*, vol. 60, 2022, Art. no. 4502215.
- [28] K. Gao, L. Huang, Y. Zheng, R. Lin, H. Hu, and T. Cladouhos, "Automatic fault detection on seismic images using a multiscale attention convolutional neural network," *Geophysics*, vol. 87, no. 1, pp. 13–29, Jan. 2022.
- [29] X.-L. Wei et al., "Seismic fault detection using convolutional neural networks with focal loss," *Comput. Geosci.*, vol. 158, Jan. 2022, Art. no. 104968.
- [30] X. Li, X. Sun, Y. Meng, J. Liang, F. Wu, and J. Li, "Dice loss for data-imbalanced NLP tasks," 2019, *arXiv:1911.02855*.
- [31] J. Wang, J.-H. Zhang, J.-L. Zhang, F.-M. Lu, R.-G. Meng, and Z. Wang, "Research on fault recognition method combining 3D Res-UNet and knowledge distillation," *Appl. Geophys.*, vol. 18, no. 2, pp. 199–212, Nov. 2021.
- [32] R. Feng, D. Grana, and N. Balling, "Uncertainty quantification in fault detection using convolutional neural networks," *Geophysics*, vol. 86, no. 3, pp. 41–48, Mar. 2021.
- [33] H. Di, C. Li, S. Smith, Z. Li, and A. Abubakar, "Imposing interpretational constraints on a seismic interpretation convolutional neural network," *Geophysics*, vol. 86, no. 3, pp. 63–71, May 2021.
- [34] M. Z. Alom, M. Hasan, C. Yakopcic, T. M. Taha, and V.K. Asari, "Recurrent residual convolutional neural network based on U-Net (R2U-Net) for medical image segmentation," 2018, *arXiv:1802.06955*.
- [35] D. D. Kadia, M. Z. Alom, R. Burada, T. V. Nguyen, and V.K. Asari, "R²U3D: Recurrent residual 3D U-Net for lung segmentation," *IEEE Access*, vol. 9, pp. 88835–88843, 2021.
- [36] D. M. Hawkins, "The problem of overfitting," *J. Chem. Inf. Comput. Sci.*, vol. 44, no. 1, pp. 1–12, Dec. 2003.
- [37] R. Ranjbarzadeh, A. B. Kasgari, S. J. Ghoushchi, S. Anari, M. Naseri, and M. Bendechache, "Brain tumor segmentation based on deep learning and an attention mechanism using MRI multi-modalities brain images," *Sci. Rep.*, vol. 11, no. 1, pp. 1–17, May 2021.
- [38] H. Liu et al., "Rock thin-section analysis and identification based on artificial intelligent technique," *Petroleum Sci.*, vol. 19, no. 4, pp. 1605–1621, Aug. 2022.
- [39] K. He, X. Zhang, S. Ren, and J. Sun, "Deep residual learning for image recognition," in *Proc. IEEE Conf. Comput. Vis. Pattern Recognit. (CVPR)*, Jun. 2016, pp. 770–778.
- [40] S.-B. Zhang, H.-J. Si, X.-M. Wu, and S.-S. Yan, "A comparison of deep learning methods for seismic impedance inversion," *Petroleum Sci.*, vol. 19, no. 3, pp. 1019–1030, Jun. 2022.
- [41] C. Shorten and T. M. Khoshgoftaar, "A survey on image data augmentation for deep learning," *J. Big Data*, vol. 6, no. 1, pp. 1–48, Jul. 2019.
- [42] P. Domingos, "Bayesian averaging of classifiers and the overfitting problem," in *Proc. ICML*, 2000, pp. 223–230.
- [43] A. Krizhevsky, I. Sutskever, and G. E. Hinton, "ImageNet classification with deep convolutional neural networks," *Commun. ACM*, vol. 60, no. 6, pp. 84–90, May 2017.
- [44] C. H. Sudre, W. Li, T. Vercauteren, S. Ourselin, and M. Jorge, "Generalised dice overlap as a deep learning loss function for highly unbalanced segmentations," in *Deep Learning in Medical Image Analysis and Multimodal Learning for Clinical Decision Support*. New York, NY, USA: ACM, 2017, pp. 240–248.
- [45] S. Xie and Z. Tu, "Holistically-nested edge detection," in *Proc. IEEE Int. Conf. Comput. Vis. (ICCV)*, Dec. 2015, pp. 1395–1403.
- [46] D. P. Kingma and J. Ba, "Adam: A method for stochastic optimization," 2014, *arXiv:1412.6980*.



Xiao Ma received the B.S. degree in applied geophysics from the Chengdu University of Technology, Chengdu, China, in 2020. He is currently pursuing the M.S. degree with the China University of Petroleum (Beijing), Beijing, China.

He joined the WaveTomo Group led by Prof. Gang Yao, China University of Petroleum (Beijing). His main research interests include deep learning and its application on seismic data interpretation and processing. He is currently focusing on seismic faults detection and seismic data denoise with deep learning methods.



Gang Yao (Member, IEEE) received the B.S. and M.S. degrees in geophysics from the China University of Geosciences (Beijing), Beijing, China, in 2005 and 2008, respectively, and the Ph.D. degree in geophysics from Imperial College London, London, U.K., in 2013.

He was a Research Associate of the FULLWAVE Consortium led by Prof. Michael Warner, Imperial College London, from 2013 to 2017. He was a Post-Doctoral Research Fellow with Rice University, Houston, TX, USA, in 2018. He was appointed as Associate Professor and then Full Professor with the China University of Petroleum (Beijing), Beijing, where he set up the WaveTomo Group. His main research interests are on seismic signal processing, imaging, inversion, and artificial intelligence for seismic data processing.

Dr. Yao is a member of EAGE and SEG. He is an Associate Editor of *Petroleum Science* and *Chinese Journal of Geophysics*.



Feng Zhang received the B.S. degree in electrical and mechanical engineering from the Beijing Institute of Technology, Beijing, China, in 2005, the M.S. degree in signal processing and communications from Edinburgh University, Edinburgh, U.K., in 2006, and the Ph.D. degree in reservoir geophysics from Imperial College London, London, U.K., in 2010.

He was a Post-Doctoral Research Associate with British Geological Survey, Edinburgh, from 2010 to 2011. He joined the China University of Petroleum (Beijing), Beijing, in 2011, where he is currently a Professor. His research interests include seismic inversion, rock physics, and multicomponent seismic and seismic anisotropy.

Dr. Zhang is an Associate Editor of the *Journal of Geophysics and Engineering* and *Petroleum Science*. He is also a member of EAGE and SEG.



Di Wu received the B.S. degree in physics from Shanxi University, Taiyuan, China, in 2005, the M.S. degree in geophysics from the Institute of Geology and Geophysics, Chinese Academy of Sciences, Beijing, China, in 2008, and the Ph.D. degree in geophysics from Imperial College London, London, U.K., in 2013.

She then worked as a Geophysicist with PGS London Branch, London. In 2015, she joined the China University of Petroleum (Beijing), Beijing, and was promoted as Associate Professor of Geophysics. Her main research interests are in seismic data processing and migration imaging.

Dr. Wu is a member of EAGE and SEG.